# A Density-Functional Study of the Mechanism for the Diastereoselective Epoxidation of Chiral Allylic Alcohols by the Titanium Peroxy Complexes

Meng Cui,[†] Waldemar Adam,*[,‡] Jian Hua Shen,[†] Xiao Min Luo,[†] Xiao Jian Tan,[†] Kai Xian Chen,[†] Ru Yun Ji,[†] and Hua Liang Jiang*[,†]

*Center for Drug Design and Discovery and the State Key Laboratory of New Drug Research, Shanghai Institute of Materia Medica, Shanghai Institutes for Biological Sciences, Chinese Academy of Sciences, Shanghai 200031, P. R. China, and Institut für Organische Chemie, Universität of Würzburg, Am Hubland, D-97074, Würzburg, Germany*

*jiang@iris3.simm.ac.cn*

*Received August 8, 2001*

The epoxidation of three stereolabeled methyl-substituted chiral allylic alcohols with $^{1,2}$A and/or $^{1,3}$A allylic strain, namely 3-methylbut-3-en-2-ol (**1a**), pent-3-en-2-ol (**1b**), and 3-methylpent-3-en-2-ol (**1c**), have been studied by the density-functional theory method, B3LYP/6-31+G(d,p). For each substrate we calculated the two prereaction complexes with $Ti(OH)_4$/MeOOH (the oxidant model for $Ti(O\text{-}i\text{-}Pr)_4$/*t*-BuOOH), their *threo* and *erythro* transition states for oxygen transfer, and the corresponding product complexes. For substrate **1a**, the *erythro* transition state is 0.91 kcal/mol of lower energy than the *threo* one; for substrates **1b** and **1c**, the *threo* compared to the *erythro* transition states are by 1.05 and 0.21 kcal/mol more favorable, respectively. The *threo*/*erythro* product ratios have been estimated from the computed free energies for the competing *threo* and *erythro* transition states **3a**−**c** in $CH_2Cl_2$ solution to be 12:88 (**1a**), 92:8 (**1b**), and 77:23 (**1c**), which are in good accordance with the experimental values 22:78 (**1a**), 91:9 (**1b**), and 83:17 (**1c**). The diastereoselectivity of this diastereoselective oxyfunctionalization is rationalized in terms of the competition between $^{1,3}$A and $^{1,2}$A strain and the electronic advantage for the spiro transition state. In addition, solvent effects are also play a role for the diastereoselectivity at the same time.

## Introduction

The epoxidation of olefinic compounds is one of the most important and valuable reactions in organic synthesis and has recently been the subject of intensive study.[1] Of interest has been the mechanism of the oxygen transfer for the catalytic and stereoselective epoxidation, which still presents a major challenge for the experimentalist as well as theoretician.[2]

The stereoselective epoxidation has been thoroughly investigated since the discovery of the peracid epoxidation of alkenes by Prileschajew in 1909.[3] The mechanism of the oxygen transfer was elucidated already in 1950 by Bartlett, in terms of the ground-breaking "butterfly" transition structure.[4] In 1957 Henbest observed the synergistic interplay between the conformational control and substrate−reagent interaction through hydrogen bonding in the highly diastereoselective peracid epoxidation of cyclic allylic alcohols. He extended the "butterfly" transition structure to include hydrogen bonding of the allylic hydroxy group with the peroxy oxygen of the peracid.[5] In 1979, Sharpless[6] proposed that a *spiro* transition structure was more likely than a planar one in the "butterfly" mechanism. Recent theoretical work by Bach et al.,[7] by Houk et al.,[8] and by Sarzi-Amadè et al.[9] have consolidated the *spiro* transition structure for the peracid epoxidation. Since then, this valuable mechanistic concept has been extensively applied for the stereocontrolled oxyfunctionalization in organic synthesis.[10]

The above-mentioned studies have mainly focused on the peracid epoxidation of alkenes. To rationalize the experimental observations and design new catalytic systems,[11] a detailed knowledge of the transition struc-

* Please address correspondence and requests for reprints to Hua Liang Jiang, Shanghai Institute of Materia Medica, Chinese Academy of Sciences, 294 Taiyuan Road, Shanghai 200031. Phone: +86−21−64318401. Fax: +86-21-64370269. Alternate e-mail for H.-L. Jiang: hljiang@mail.shcnc.ac.cn. Also address correspondence to W. Adam: adam@chemie.uni-wuerzburg.de.

† Shanghai Institute of Materia Medica.

‡ Universität of Würzburg.

(1) *Methods of Organic Chemistry (Houben Weyl)*, 4th ed.; Helmchen, G.; Hoffmann, R. W.; Mulzer, J.; Schaumann, E., Eds.; G. Thieme: Stuttgart/New York, 1995; Vol. E21e.

(2) (a) Jorgensen, K. A. *Chem. Rev.* **1989**, *89*, 431−458. (b) Jacobsen, E. N. *Transition Metal-catalyzed Oxidations: Asymmetric Epoxidation. In Comprehensive Organometallic Chemistry II*; Wilkinson, G., Stone, F. G. A., Abel, E. W., Hegedus, L. S., Eds.; Pergamon: New York, 1995; Vol. 12, Chapter 11.1.

(3) Prileschajew, N. *Ber.* **1909**, *42*, 4811−4815.

(4) Bartlett, P. D. *Rec. Chem. Prog.* **1950**, *11*, 47−51.

(5) Henbest, H. B.; Wilson, R. A. L. *J. Chem. Soc.* **1957**, 1958−1965.

(6) Sharpless, K. B.; Verhoeven, T. R. *Aldrichim. Acta* **1979**, *12*, 63−74.

(7) (a) Bach, R. D.; Estévez, C. M.; Winter, J. E.; Glukhoutsev, M. N. *J. Am. Chem. Soc.* **1998**, *120*, 680−685. (b) Bach, R. D.; Glukhovtsev, M. N.; Gonzalez, C. *J. Am. Chem. Soc.* **1998**, *120*, 9902−9910. (c) Bach, R. D.; Winter, J. E.; McDouall, J. *J. Am. Chem. Soc.* **1995**, *117*, 8586. (d) Bach, R. D.; Ayala, P. Y.; Schlegel, H. B. *J. Am. Chem. Soc.* **1996**, *118*, 12758−12765.

(8) (a) Singleton, D. A.; Merrigan, S. R.; Liu, J.; Houk, N. K. *J. Am. Chem. Soc.* **1997**, *119*, 3385−3386. (b) Houk, K. N.; Liu, J.; DeMello, N. C.; Condroski, K. R. *J. Am. Chem. Soc.* **1997**, *119*, 10147−10152.

(9) (a) Freccero, M.; Gandolfi, R.; Sarzi-Amadè, M.; Rastelli, A. *J. Org. Chem.* **1999**, *64*, 3853−3860. (b) Freccero, M.; Gandolfi, R.; Sarzi-Amadè, M.; Rastelli, A. *J. Org. Chem.* **2000**, *65*, 2030−2042.

(10) Hoveyda, A. H.; Evans, D. A.; Fu, C. G. *Chem. Rev.* **1993**, *93*, 1307−1370.

(11) Collman, J. P.; Zhang, X.; Lee, V. J.; Uffelman, E. S.; Brauman, J. I. *Science* **1993**, *261*, 1404−1411.

10.1021/jo016015c CCC: $22.00 
Published on Web 02/06/2002

**Scheme 1. The Codification of the Allylic Alcohols 1, Prereaction Complexes 2, Transition Structures 3, and Product Complexes 4 and the Diastereomeric Ratios for the Epoxidation of the Chiral Allylic Alcohols 1 by Ti(O-i-Pr)$_4$/t-BuOOH**[a]

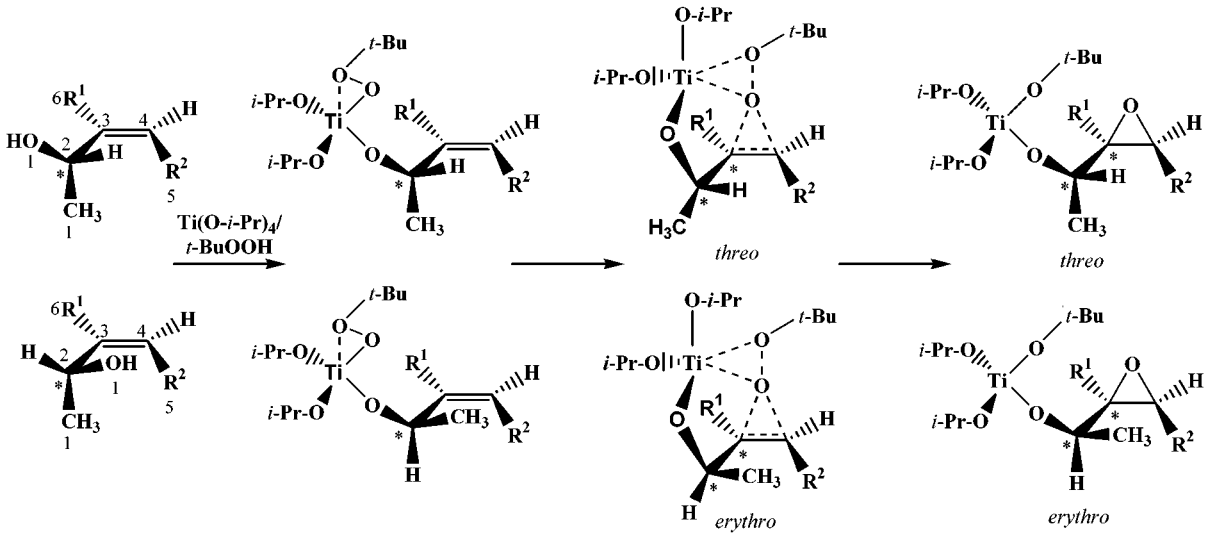


| $R^1$ | $R^2$ | | | | | *threo* | *erythro* | 2*S*,3*R* | 2*R*,3*R* | *threo* : *erythro* |
|---|---|---|---|---|---|---|---|---|---|---|
| $CH_3$ | H | 2*S*-**1a** | 2*R*-**1a** | 2*S*-**2a** | 2*R*-**2a** | (2*S*, 3*S*)-**3a** | (2*R*, 3*S*)-**3a** | (2*S*, 3*S*)-**4a** | (2*R*, 3*S*)-**4a** | **22 : 78** |
| H | $CH_3$ | 2*S*-**1b** | 2*R*-**1b** | 2*S*-**2b** | 2*R*-**2b** | (2*S*, 3*S*)-**3b** | (2*R*, 3*S*)-**3b** | (2*S*, 3*S*)-**4b** | (2*R*, 3*S*)-**4b** | **91 : 09** |
| $CH_3$ | $CH_3$ | 2*S*-**1c** | 2*R*-**1c** | 2*S*-**2c** | 2*R*-**2c** | (2*S*, 3*S*)-**3c** | (2*R*, 3*S*)-**3c** | (2*S*, 3*S*)-**4c** | (2*R*, 3*S*)-**4c** | **83 : 17** |

[a] The carbon and oxygen atoms are codified separately. The experimental *threo*:*erythro* ratios (last column) have been taken from reference 15c.

tures for the metal-catalyzed oxygen-transfer process is necessary at the molecular level, for which present-day computational chemistry is well-suited. Recent computational work of N. Rösch et al.,[12] Frenking et al.,[13] and Wu et al.[14] shed light on the transition structures of metal-catalyzed oxyfunctionalizations.

Recently, Adam et al. have investigated the diastereoselective epoxidation of chiral acyclic allylic alcohols, with stoichiometric and catalytic oxidants, which has provided valuable mechanistic information on the transition-state geometries of such oxyfunctionalizations.[15] In this paper, the allylic alcohols 3-methylbut-3-en-2-ol (**1a**), pent-3-en-2-ol (**1b**), and 3-methylpent-3-en-2-ol (**1c**) have been introduced as stereochemical probes to assess transition structures in oxygen-transfer reactions (Scheme 1). In these substrates, the derivative **1a** probes for the importance of 1,2-allylic strain ($^{1,2}$A, i.e., the steric repulsion between the $C_1$ and $C_6$ ($\mathbf{R}^1$) methyl groups), **1b** tests for the 1,3-allylic strain ($^{1,3}$A, i.e., the steric repulsion between the $C_1$ and $C_5$ ($\mathbf{R}^2$) methyl groups), and in substrate **1c** the $^{1,2}$A and $^{1,3}$A strains are in competition with one another.

**Scheme 2. Ligand Exchange in the Epoxidation of the Chiral Allylic Alcohols 1 by the Titanium Peroxy Complex**[a]

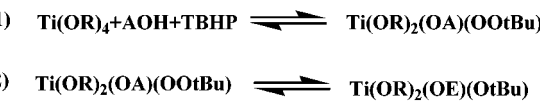


For the Ti(O-*i*-Pr)$_4$/*t*-BuOOH oxidant of the Sharpless–Katsuki epoxidation,[16] the titanium(IV) metal rapidly exchanges its isopropoxide ligands for the *tert*-butyl hydroperoxide. The latter is coordinatively activated for oxygen transfer through its enhanced electrophilic character. Also, the allylic alcohol is bound by ligand exchange to the titanium metal to afford the so-called "loaded complex" or metal template (step 1, Scheme 2), the latter transfers the activated oxygen atom to the C=C double bond and the epoxidized product forms (step 2, Scheme 2); further exchange maintains the catalytic cycle.

(12) (a) Rösch, N.; Gisdakis, P.; Yudanov, I. V.; Valentin, C. D. In *DFG Research Report on Peroxide Chemistry: Mechanistic and Preparative Aspects of Oxygen Transfer*; Adam, W., Ed; Wiley-VCH: Weinheim, 2000; pp 601–619. (b) Yudanov, I. V.; Gisdakis, P.; valentin, C. D.; Rösch, N. *Eur. J. Inorg. Chem.* **1999**, 2135–2145. (c) Gisdakis, P.; Antonczak, S.; Köstlmeier, S.; Herrmann, W. A.; Rösch, N. *Angew. Chem., Int. Ed.* **1998**, *37*, 2211–2214. (d) Valentin, C. D.; Gandolfi, R.; Gisdakis, P.; Rösch, N. *J. Am. Chem. Soc.* **2001**, *123*, 2365–2376.

(13) (a) Deubel, D. V.; Sundermeyer, J.; Frenking, G. *Org. Lett.* **2001**, *3*, 329–332. (b) Torrent, M.; Sola M.; Frenking G. *Chem. Rev.* **2000**, *100*, 439–493.

(14) (a) Wu, Y. D.; Lai D. K. W. *J. Am. Chem. Soc.* **1995**, *117*, 11327–11336. (b) Wu, Y. D.; Lai D. K. W. *J. Org. Chem.* **1995**, *60*, 673–680. (c) Wu, Y. D.; Sun, J. *J. Org. Chem.* **1998**, *63*, 1752–1753.

(15) (a) Adam, W.; Wirth, T. *Acc. Chem. Res.* **1999**, *32*, 703–710. (b) Adam, W.; Smerz, A. K. *J. Org. Chem.* **1996**, *61*, 3506–3510. (c) Adam, W.; Kumar, R.; Reddy, T. I.; Renz, M. *Angew. Chem, Int. Ed. Engl.* **1996**, *35*, 880–882. (d) Adam, W.; Mitchell, C. M.; Saha-Möller, C. R. *Eur. J. Org. Chem.* **1999**, 785–790. (e) Adam, W.; Stegmann, V. R.; Saha-Möller, C. R. *J. Am. Chem. Soc.* **1999**, *121*, 1879–1882. (f) Adam, W.; Degen, H.-G.; Saha-Möller, C. R. *J. Org. Chem.* **1999**, *64*, 1274–1277. (g) Adam, W.; Mitchell, C. M.; Saha-Möller, C. R.; Weichold, O. In *Metal-Oxo and Metal-Peroxo Species in Catalytic Oxidations for Structure and Bonding*; Meunier, B.; Ed.; Springer-Verlag: Berlin-Heidelberg-New York-Tokyo, 2000; pp 237–285.

(16) (a) Woodard, S. S.; Finn, M. G.; Sharpless, K. B. *J. Am. Chem. Soc.* **1991**, *113*, 106–113. (b) Ito, Y. N.; Katsuki, T. *Bull. Chem. Soc. Jpn.* **1999**, *72*, 603–619.

The $O_1-C_2-C_3-C_4$ (α) dihedral angle (Scheme 1) in the transition state for the allylic alcohol epoxidation is critical for whether *threo* or *erythro* diastereoselectivity prevails in the oxygen transfer.[15a] For the *m*-chloroperbenzoic acid (*m*-CPBA) transition state, the dihedral angle (α) has been empirically estimated to be ca. 120°, for $VO(acac)_2$/*t*-BuOOH between 40° and 50°, and for Ti(O-*i*-Pr)$_4$/*t*-BuOOH between 70° and 90°. The obtuse dihedral angle of ca. 120° in the case of *m*-CPBA is favorable for substrate−oxidant hydrogen bonding and results in *threo* diastereoselectivity, which is conditioned by minimal $^{1,3}$A strain. A recent computational investigation on the 3-methylbut-3-en-2-ol (**1a**), pent-3-en-2-ol (**1b**), and 3-methylpent-3-en-2-ol (**1c**) epoxidation by performic acid shows that the transition structures of **1a** for the *threo* (α −124.6°) geometry is less favorable than for the *erythro* (α 20.8°) by 0.96 kcal/mol; the transition structures of **1b** for the *threo* (α −135.3°) is more stable than that for the *erythro* (α 34.4°) by 1.70 kcal/mol;[9b] the transition structures of **1c** for the *threo* (α 130.5°) geometry is more favorable than that for *erythro* (α 34.7°) by 1.14 kcal/mol.[17]

In this paper we report a density-functional theory (DFT) computational study of the transition structures for the epoxidation of the methyl-substituted chiral allylic alcohols **1a**−**c** by the titanium peroxy complexes (Scheme 1). The present computational results show that the metal-alcoholate bonding plays a decisive role in the diastereoselective epoxidation of the allylic alcohols **1a**−**c** on account of the compromise between steric repulsion and electronic effects in the metal template.

## The Computational Method

The actual Ti(O-*i*-Pr)$_4$/*t*-BuOOH oxidant is too large to be calculated with the more accurate computational methods, so we simplified this oxidation system by replacing the *tert*-butyl group of *t*-BuOOH by a methyl group and the propyl ligands of Ti(O-*i*-Pr)$_4$ by hydrogen atoms which is the same with the model of previous studies proposed by Yudanov et al.[12(b)] This simplified $Ti(OH)_4$/MeOOH oxidant is suitable to be computed with higher-level computational methods, e.g., ab initio and density-functional-theory (DFT) methods. The codification of the substrate molecules is given in Scheme 1.

The computations were carried out by the Gaussian 98 program,[18] by using the B3LYP nonlocal density functional approximation,[19] which employs the Lee−Yang−Parr correlation functional,[20] combined with the Becke three-parameter hybrid exchange functional.[21] This method has been shown to give quite good results for transition structures involving transition metals.[12−14] The geometrical optimizations were carried out with the 6-31+G(d,p) basis set. In addition, the basis set may affect the optimized structures and energies of molecules with transition metals, and Frenking et al. demonstrated that the core and valence electrons of the transition metals should be considered in the basis sets to obtain reliable geometries and energies.[13b] Accordingly, we have employed the 6-31+G(d,p) basis set in our structure optimization and energy calculation. The stationary and transitional points on the potential energy surfaces were characterized by the calculation of the vibrational frequencies at the B3LYP/6-31+G(d,p) level, as well as the zero-point energies (ZPE) and thermal corrections. Solvent effects were determined by employing the Conductor-like Screening model (COSMO).[22] The default solvent model COSMO and a dielectric constant of $\epsilon$ 8.9 were used to simulate methylene chloride ($CH_2Cl_2$) as solvent system.

## Results and Discussions

**Conformational Search of the Substrates.** For the allylic alcohol **1a**−**c**, a conformational search was performed at the level of B3LYP/6-31+G(d,p) about the $C_2-C_3$ bond. The $O_1-C_2-C_3-C_4$ dihedral angle (denoted α throughout this paper) was changed from 0 to 180° in increments of 10°; for each conformer (at a fixed α) the structure was fully optimized by using B3LYP/6-31+G(d,p). Since each substrate has two enantiomers, namely 2*R* and 2*S*, the energy for the 2*S* configuration at a dihedral angle α of A is equivalent to the energy for the 2*R* configuration with a dihedral angle α of 360-A. Thus, by the combination of the potential energies of the 2*R* and 2*S* enantiomers from 0 to 180°, the energy profile for the substrate is obtained for the α angle from 0 to 360° (Figures 1−3).

The energy profile of the conformational search for substrate **1a** is presented in Figure 1a, from which three local minimum-energy conformers of **1a** are evident. For these three local minimum-energy conformers of the 2*S* configuration, the dihedral angles α are at about −20°, 120°, and −125°; those for the 2*R* configuration are located at about 20°, −120°, and 125°. To simplify following discussion, we assign *S* and *R* as not only the intrinsic configurations but also the global-minimum energy and second lowest-energy conformations of each substrate, respectively. According this definition, the global minimum energy conformation of **1a** is represented as 2*S*-**1a** (α ca. 120° for 2*S* configurations), and the second lowest-energy conformation is represented as 2*R*-**1a** (α ca. 20° for 2*R* configuration). Full geometric optimization was performed on 2*S*-**1a** and 2*R*-**1a** at the B3LYP/6-31+G(d,p) level. The optimized structures of 2*S*-**1a** and 2*R*-**1a** are presented in Figure 1b, with accurate α values of 117.3° for 2*S*-**1a** and 16.8° for 2*R*-**1a**. In the gas phase, 2*S*-**1a** is by 0.53 kcal/mol of lower energy than 2*R*-**1a** comparing with the previous computational results 0.48 kcal/mol.[9b]

In a similar way, the potential energy profiles as a function of the α angle of the substrates **1b** and **1c** were obtained (Figures 2 and 3). For substrate **1b**, the global minimum-energy conformer 2*S*-**1b** is by 2.28 kcal/mol of lower energy than the second lowest-energy conformer 2*R*-**1b** comparing with the previous computational results 2.32 kcal/mol.[9b] The optimized B3LYP/6-31+G(d,p) structures give α angles of 120.4 and 35.7° for 2*S*-**1b** and 2*R*-**1b**, respectively. For substrate **1c** the global minimum-energy conformer 2*S*-**1c** is by 1.39 kcal/mol lower in

(17) Adam, W.; Bach, R. D.; Dmitrenko, O.; Saha-Moller, C. R. *J. Org. Chem.* **2000**, *65*, 6715−6728.
(18) Frisch, M. J.; Trucks, G. W.; Schlegel, H. B.; Scuseria, G. E.; Robb, M. A.; Cheeseman, J. R.; Zakrzewski, V. G.; Jr., J. A. M.; Stratmann, R. E.; Burant, J. C.; Dapprich, S.; Millam, J. M.; Daniels, A. D.; Kudin, K. N.; Strain, M. C.; Farkas, O.; Tomasi, J.; Barone, V.; Cossi, M.; Cammi, R.; Mennucci, B.; Pomelli, C.; Adamo, C.; Clifford, S.; Ochterski, J.; Petersson, G. A.; Ayala, P. Y.; Cui, Q.; Morokuma, K.; Malick, D. K.; Rabuck, A. D.; Raghavachari, K.; Foresman, J. B.; Cioslowski, J.; Ortiz, J. V.; Baboul, A. G.; Stefanov, B. B.; Liu, G.; Liashenko, A.; Piskorz, P.; Komaromi, I.; Gomperts, R.; Martin, R. L.; Fox, D. J.; Keith, T.; Al-Laham, M. A.; Peng, C. Y.; Nanayakkara, A.; Gonzalez, C.; Challacombe, M.; Gill, P. M. W.; Johnson, B.; Chen, W.; Wong, M. W.; Andres, J. L.; Gonzalez, C.; Head-Gordon, M.; Replogle, E. S.; Pople, J. A.; A.7 ed.; Gaussian, Inc.: Pittsburgh, PA, 1998.
(19) Stephens, P. J.; Devlin, F. J.; Chablowski, C. F.; Frisch, M. J. *J. Phys. Chem.* **1994**, *98*, 11623−11627.
(20) Lee, C.; Yang, W.; Parr, R. G. *Phys. Rev. B* **1988**, *37*, 785−789.
(21) (a) Becke, A. D. *Phys. Rev. A* **1988**, *38*, 3098−3100. (b) Becke, A. D. *J. Chem. Phys.* **1993**, *98*, 5648−5652.
(22) Barone, V.; Cossi, M.; Tomasi, J. *J. Phys. Chem. A* **1998**, *102*, 1995−2001.

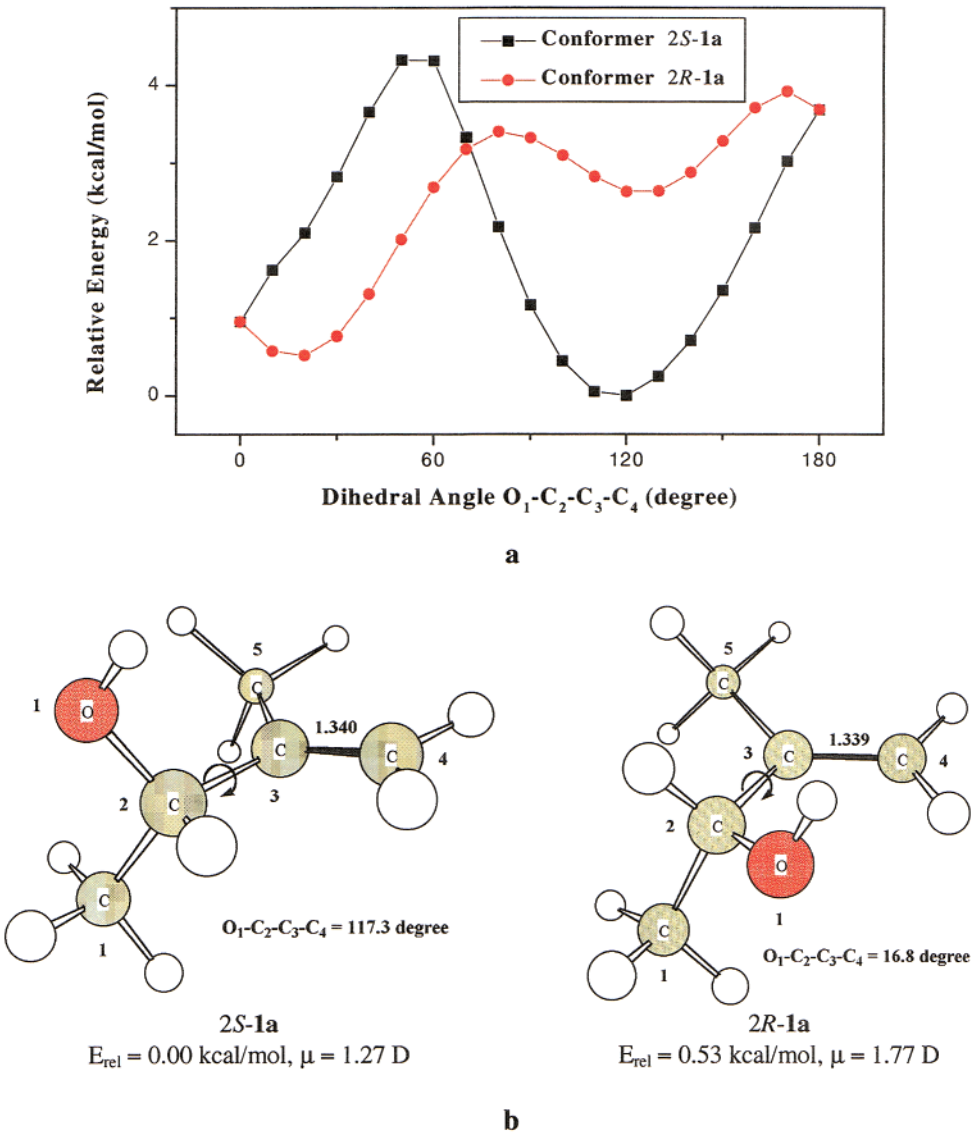


**Figure 1.** Optimization of the substrate conformer **1a**: (a) The energy profile as a function of the dihedral angle; (b) optimized structures and the main characteristic parameters for the first two lowest-energy conformers 2*S*-**1a** and 2*R*-**1a**; the carbon and oxygen atoms are numbered separately.

energy than the second minimum-energy conformer 2*R*-**1c**, which is well in agreement with the results of the B3LYP/6-311+G(d,p) (1.40 kcal/mol).[17]

The potential-energy profiles as a function of the α angle disclose that the rotational energy barriers about the $C_2-C_3$ bond are about 4.4 kcal/mol for substrate **1a** (Figure 1a), 5.5 kcal/mol for **1b** (Figure 2a), and 6.5 kcal/mol for **1c** (Figure 3a). This indicates that each of the local minimum-energy conformers of the substrates **1a**−**c** are attached to the Ti(O-*i*-Pr)$_4$/*t*-BuOOH oxidant, the starting point to form a substrate−oxidant template (prereaction complex). From Figures 1−3, we can find that the lowest-energy geometries ($0° < \alpha < 180°$) of these substrates 2*S*-**1a** to **c** correspond structurally to the *threo* transition structures, while the second lowest-energy conformations 2*R*-**1a** to **c** correspond to the *erythro* transition structures.

As already pointed out in the Introduction, the $O_1-C_2-C_3-C_4$ dihedral angle (α) of these chiral allylic alcohols is decisive for their diastereoselectivity. Previous computations reveal that the transition structures for the metal-catalyzed epoxidation of allylic alcohols favor the *spiro* geometry over the planar one, and the α angles for the *spiro* transition states are about 40°.[6, 10,14(b)] Wu et al. found that the *spiro* transition structure is about 3 kcal/mol of lower energy than a planar one.[14b] From Figure 1a we may notice that on rotation about the $C_2-C_3$ bond, the energy of the 2*S*-**1a** conformer will increase by about 3.7 kcal/mol to overcome a 4.4 kcal/mol energy barrier at α 40°, which is caused by $^{1,2}$A strain in the *spiro* transition structure. In contrast, the 2*R*-**1a** conformer decreases first by 0.8 kcal/mol at about α 20°, while at about 40° the 2*R*-**1a** configuration is ca. 2.3 kcal/mol lower than 2*S*-**1a**. We may conclude that the *spiro* transition state for the 2*R*-**1a** enantiomer is more favorable than 2*S*-**1a** and, thus, the *erythro* epoxidation product dominates, in agreement with the experimental results.[15c]

The conformational energies of the 2*S*-**1b** and 2*R*-**1b** enantiomers (Figure 2a) are almost the same at α 40°; however, 2*S*-**1b** possesses about 2.2 kcal/mol energy lower than 2*R*-**1b** at the local minima conformations**.** For substrate **1c**, enantiomer 2*S*-**1c** lies about 2.3 kcal/mol above 2*R*-**1c** for the 40° conformation; in fact, this α value

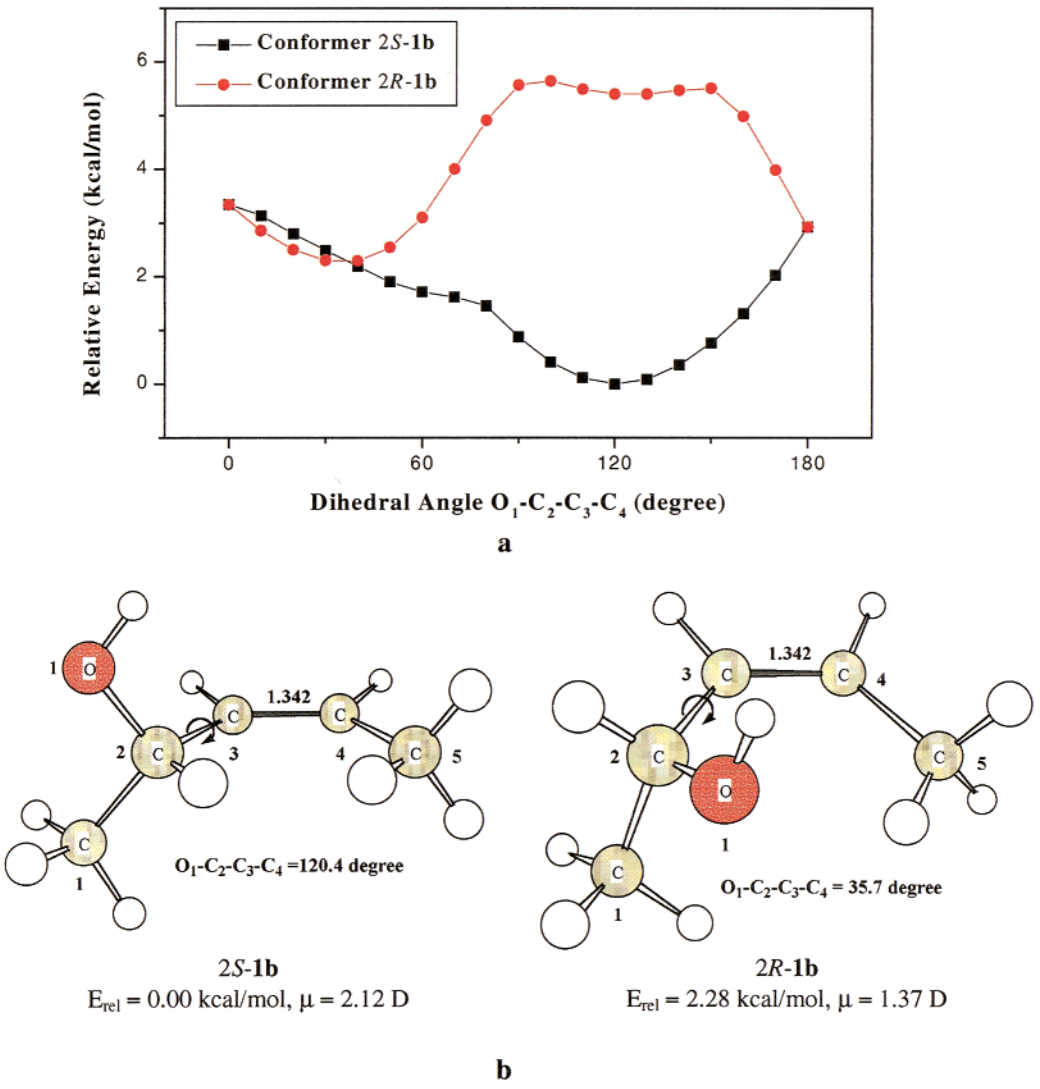


**Figure 2.** Optimization of the substrate conformer **1b**: (a) The energy profile as a function of the dihedral angle; (b) optimized structures and the main characteristic parameters for the first two lowest-energy conformers 2*S*-**1b** and 2*R*-**1b**; the carbon and oxygen atoms are numbered separately.

corresponds to the minimum-energy conformer for 2*R*-**1c**. Therefore, for the allylic alcohols **1b** and **1c**, it is hard to predict which products will be favored based only on the conformational analysis of the substrates. The structural features and energy parameters of the transition states rather than the ground-state substrates must be used to acquire reliable results, as will become evident in the later sections.

**Transition Structures.** As already addressed in the Introduction, according to the epoxidation mechanism proposed by Sharpless[16a] for the Ti(O-*i*-Pr)$_4$/*t*-BuOOH oxidant, first the exchange of the alkoxide ligands of the titanium(IV) catalyst by the allylic alcohol and the *tert*-butyl hydroperoxide (TBHP) generates the "loaded" complex (Scheme 2). The six "loaded" or prereaction complexes are derived from the minimum-energy geometries for the two 2*S* and 2*R* enantiomers of the three allylic alcohols **1a**−**c** in their optimized conformational geometries (Figures 1−3). The structures, relative energies, and dipole moments of these prereaction complexes are available in Supporting Information (Table S1 and Figure S1).

On the basis of the geometries of the allylic alcohols **1** (Figures 1−3) and the prereaction complexes **2** obtained above and the transition structural models proposed by Wu el al.,[14] we propose six possible transition structures for the oxygen transfer in the expoxidation (Figure 4). All transition structures were fully optimized by using the Synchronous Transit-Guided Quasi-Newton (STQN)[23] method at the B3LYP/6-31+G(d,p) computational level. The frequency calculations showed that all these optimized structures are true transition states with one imaginary frequency corresponding to the vibration for the oxygen transfer.

The Ti−$O_3$ bond of these transition structures **3** (Figure 4) is shortened compared to their prereaction complexes **2** (Figure S1), while the Ti−$O_2$ and $O_2$−$O_3$ bonds are lengthened. The Ti−$O_2$ and Ti−$O_3$ bond lengths are nearly equal to 2.0 Å, and that of the $O_2$−$O_3$ bond about 1.8 Å and almost perpendicular to the plane of C=C $\pi$ bond. The $O_2$−$C_3$ and $O_2$−$C_4$ bond lengths are also about 2.0 Å. The transition structures that produce the *erythro* products have a more pronounced *spiro* preference ($\alpha$ is close to 40°) than those produce the *threo* products, such that this electronic effect should favor in energy the

(23) (a) Peng, C.; Ayala, P. Y.; Schlegel, H. B.; Frisch, M. J. *J. Comput. Chem.* **1996**, *17*, 49−56. (b) Peng, C.; Schlegel, H. B. *Isr. J. Chem.* **1994**, *33*, 449−454.

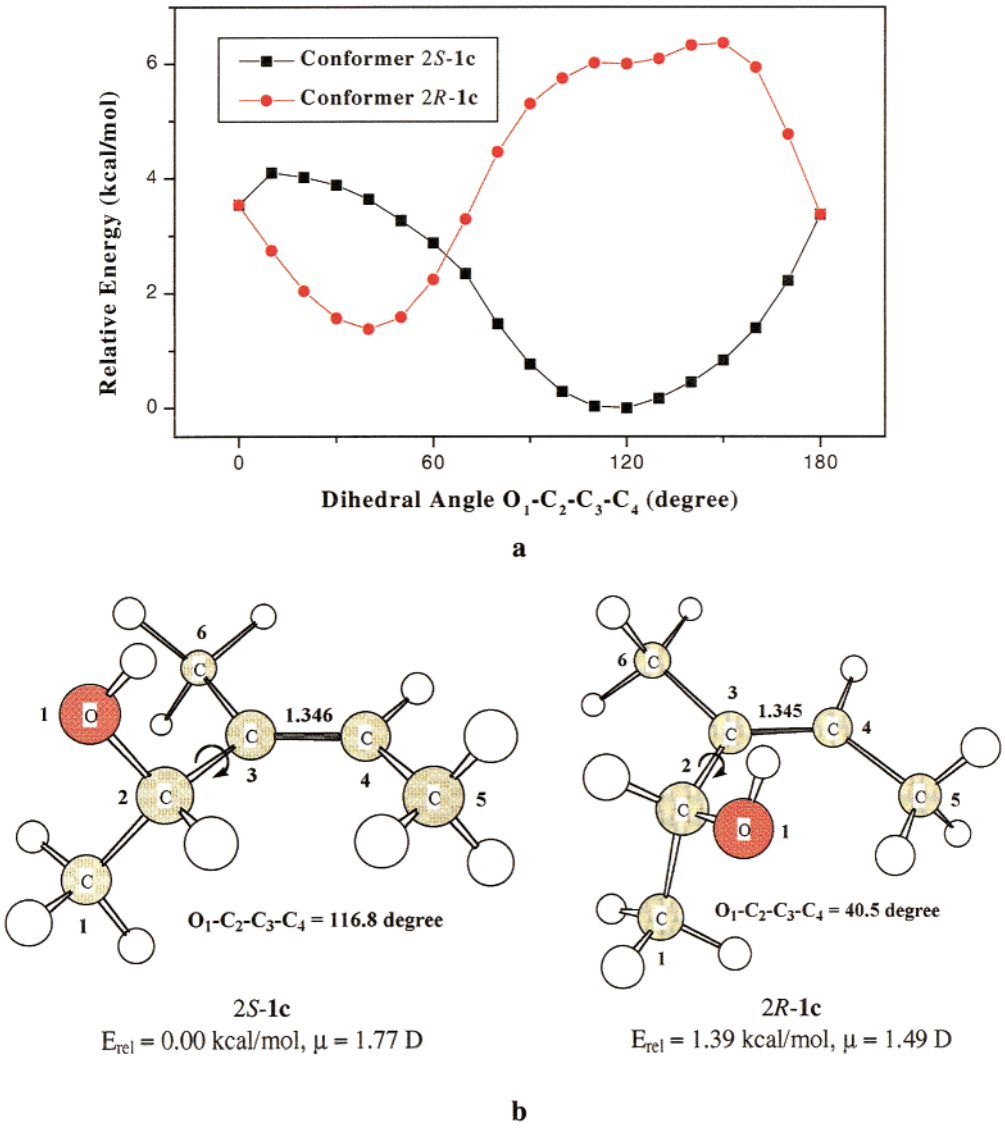


**Figure 3.** Optimization of the substrate conformer **1c**: (a) The energy profile as a function of the dihedral angle; (b) optimized structures and the main characteristic parameters for the first two lowest-energy conformers 2*S*-**1c** and 2*R*-**1c**; the carbon and oxygen atoms are numbered separately.

former transition structures over the latter. However, for most of the *threo* transition structures the steric repulsions are lower than for the *erythro* ones, such that the resulting stereoselectivity is the best compromise of these two opposing trends.

To illustrate structurally the *spiro* electronic effect,[14b] we introduce an angle $\varphi$, which is defined as the cross angle of the cross line of planes Ti−$O_2$−$O_3$ and $C_2$−$C_3$−$C_4$ with $C_3$−$C_4$ bond (Figure 4). Thus, the ideal *spiro* transition structure possesses a $\varphi$ of 90°, while for the planar geometry it is 0°. The values for the $\varphi$ and α dihedral angles of the transition structures **3** are also specified in Figure 4.

To be noted in Figure 4 is the fact that the α angles of the *threo* (2*S*,3*S*) transition structures **3** deviate significantly from those of their corresponding minimum-energy conformations of the allylic alcohol substrates **1** (Figure 1), while for the *erythro* (2*R*,3*S*) structures the differences are less pronounced. This may be rationalized in terms of the compromise between the steric repulsion and the *spiro* electronic effect. The α angle of the (2*S*,3*S*) -**3a** transition structure is 96.1°, which is by 21.2° less obtuse compared to its lower-energy conformer 2*S*-**1a** and will cost about 1.2 kcal/mol in energy due to $^{1,2}$A strain. The $\varphi$ angle is 36.2°, which deviates by 53.8° from the ideal *spiro* structure and will further increase the energy of the (2*S*,3*S*)-**3a** transition structure. In contrast, for the (2*R*,3*S*)-**3a** transition structure, the α angle is 35.6°, which is by 18.8° more obtuse than for the lower-energy conformer 2*R*-**1a** of the corresponding allylic alcohol and will again introduce about 0.5 kcal/mol more energy. A nearly ideal *spiro* structure is achieved, as may be seen from the $\varphi$ value of 78.2°, which is quite close to the optimal 90° angle. The favorable *spiro* electronic effect lowers the energy of the (2*R*,3*S*)-**3a** transition structure by 0.91 kcal/mol compared to (2*S*,3*S*) -**3a**. Correction for the solvent effect (COSMO model) in $CH_2Cl_2$ between these two transition structures provides a difference in the activation free energies of 1.17 kcal/mol in favor of the (2*R*,3*S*)-**3a** structure (Table 1). This indicates that the *spiro* electronic effect dictates the dominance of the *erythro* product of substrate **1a**, as observed experimentally (Scheme 1); that is, the *threo*:*erythro* product ratio is 22:78.[15c]

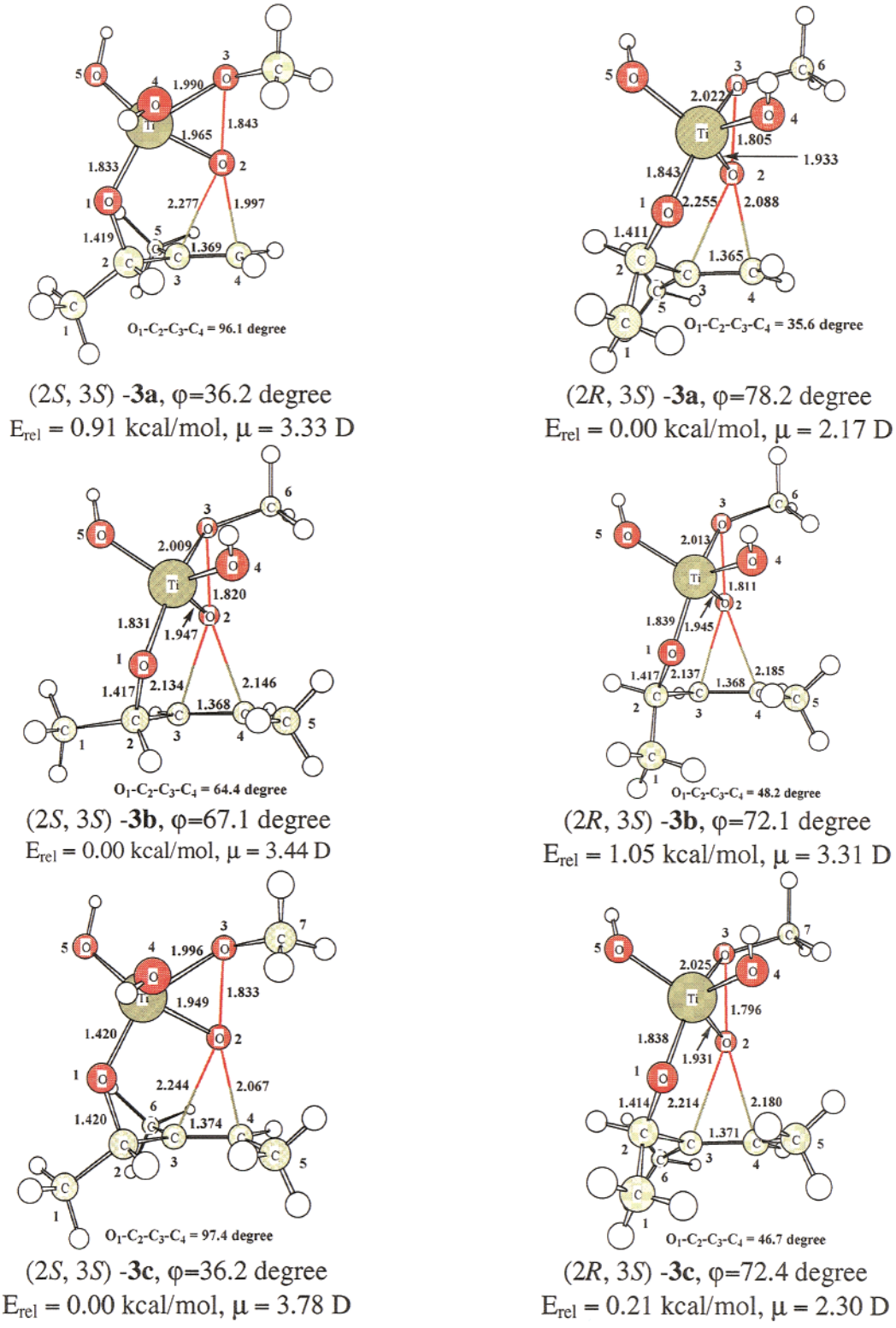


**Figure 4.** The optimized geometries of the transition structures **3** in the epoxidation of the substrates **1**; the carbon and oxygen atoms are numbered separately.

For the (2*S*,3*S*)-**3b** transition structure, the optimized B3LYP/6-31+G(d,p) level results an α angle of 64.4° (Figure 4), which diverges 56° from the lowest-energy conformation of the 2*S*-**1b** allylic alcohol substrate, and increases the energy of (2*S*, 3*S*) -**3b** by 1.6 kcal/mol (Figure 2a). The $\varphi$ angle is 67.1°, only a 22.9° deviation from the ideal *spiro* structure, which implicates that for the (2*S*,3*S*)-**3b** transition structure the *spiro* electronic effect causes only a minor destabilization. For comparison, the α angle of the (2*R*,3*S*)-**3b** transition structure is 48.2°, which deviates by only 12.5° from its lower-energy conformer of 2*R*-**1b** substrate and will increase the energy by only 0.2 kcal/mol due to $^{1,3}$A strain. The $\varphi$ angle (2*R*,3*S*)-**3b** transition structure is 72.1°, which is also quite close to the favorable *spiro* structure. On the basis of the *spiro* electronic effect, both the α and $\varphi$ angles

**Table 1. Relative Total Energies ($E_{rel}$), Enthalpies ($\Delta H$), Free Energies ($\Delta G$), and Free Energies after Solvent Correction ($\Delta G_{solv}$) between the *Threo* and *Erythro* Transition Structures 3 of the Epoxidation for the Substrates 1 (in kcal/mol)**

| transition structure | $E_{rel}$[a] | $\Delta H$[b] | $\Delta G$[c] | $\Delta G_{solv}$[d] |
|---|---|---|---|---|
| **3a** | 0.91 | 1.07 | 1.59 | 1.17 |
| **3b** | −1.05 | −1.08 | −1.54 | −1.43 |
| **3c** | −0.21 | −0.07 | −0.15 | −0.70 |

[a] The relative total energy was calculated from the total energy in Table S1 in the Supporting Information, $E_{rel} = E_{threo} - E_{erythro}$, here $E_{threo}$ and $E_{erythro}$ are, respectively, the total energies of the *threo* the *erythro* transition structures. [b] Relative gas-phase enthalpy (298 K), $\Delta H = \Delta E_{tot} + E_{corr}$, where $\Delta E_{corr}$ is the thermal correction energy difference between the *threo* and *erythro* transition states. [c] Relative free energy $\Delta G$, given as the difference of the free energies between the *threo* and *erythro* transition structures, which was computed from the results of the frequency calculation by the B3LYP/6-31+G(d,p) method. [d] Relative free energy after solvent correction with the COSMO model, $\Delta G_{solv} = \Delta G + \delta G_{solv}$, where $\delta G_{solv} = G_{solv}$(*threo*) − $G_{solv}$(*erythro*), $G_{solv}$(*threo*) and $G_{solv}$(*erythro*) are the solvent effects of the *threo* and *erythro* transition structures, respectively.

**Table 2. The Calculated Activation Energies ($\Delta E^{\ddagger}$), Activation Enthalpies ($\Delta H^{\ddagger}$), Activation Free Energies ($\Delta G^{\ddagger}$), and Solvent-Corrected Activation Free Energies ($\Delta G^{\ddagger}_{solv}$), of the Prereaction Complexes 2 to Their *Threo* and *Erythro* Epoxide Products (in kcal/mol)**

| transition structure | $\Delta E^{\ddagger}$[a] | $\Delta H^{\ddagger}$[b] | $\Delta G^{\ddagger}$[c] | $\Delta G^{\ddagger}_{solv}$[d] |
|---|---|---|---|---|
| (2*S*,3*S*)-**3a** | 18.7 | 17.4 | 20.4 | 18.5 |
| (2*R*,3*S*)-**3a** | 16.9 | 16.2 | 17.3 | 18.0 |
| (2*S*,3*S*)-**3b** | 18.6 | 17.2 | 20.7 | 19.9 |
| (2*R*,3*S*)-**3b** | 16.9 | 15.6 | 19.5 | 17.9 |
| (2*S*,3*S*)-**3c** | 16.9 | 15.5 | 18.7 | 17.1 |
| (2*R*,3*S*)-**3c** | 15.1 | 13.8 | 17.3 | 16.0 |

[a] Activation energy calculated from the total energy in Table S1 in the supporting Information, $\Delta E^{\ddagger} = E^{\ddagger}_{tot} - E_{tot}$, where $E^{\ddagger}_{tot}$ is the total energy of the transition structure **3** and $E_{tot}$ is the total energy of the prereaction complex **2**. [b] Gas-phase activation enthalpy (298 K), $\Delta H^{\ddagger} = \Delta E^{\ddagger} + \Delta E_{corr}$, where $\Delta E_{corr}$ is the thermal correction energy difference between the transition structure **3** and the prereaction complex **2**. [c] Activation free energy, which was computed from the results of the frequency calculation by the B3LYP/6-31+G(d,p) method. [d] Solvent-corrected activation free energy calculated by the COSMO model by the B3LYP/6-31+G(d,p) method; the dielectric constant was set at $\epsilon = 8.9$ to mimic the $CH_2Cl_2$ medium.

suggest that the (2*R*,3*S*)-**3b** transition structure should be preferred over the (2*S*,3*S*)-**3b** one. However, the computations reveal that the (2*S*,3*S*)-**3b** structure is by 1.05 kcal/mol of lower energy than the (2*R*,3*S*)-**3b** one (Figure 4); indeed, the free-energy difference in $CH_2Cl_2$ for these two transition states is by 1.43 kcal/mol in favor of the (2*S*,3*S*)-**3b** structure, as corrected by the COSMO solvent model (Table 1). This discrepancy arises from $^{1,3}$A strain. Figure 4 reveals that there is no $^{1,3}$A strain in the (2*S*,3*S*)-**3b** transition state, while the (2*R*,3*S*)-**3b** transition state possesses considerable $^{1,3}$A strain. The $^{1,3}$A strain may be estimated from the potential energy profile of substrate **1b** (Figure 2a). The energy difference between the two conformers of **1b** at an angle of α 64.4° for 2*S*-**1b** (corresponds to (2*S*,3*S*)-**3b** transition structure) and at an angle of α 48.2° for 2*R*-**1b** (corresponds to (2*R*,3*S*)-**3b** transition structure), amounts to 0.9 kcal/mol in favor of the 2*S*-**1b** conformer at the B3LYP/6-31+G-(d,p) level. Therefore, we can conclude that the *threo*:*erythro* ratio (91:9[15c]) in the epoxidation of substrate **1b** is dominated by $^{1,3}$A strain.

For the (2*S*,3*S*)-**3c** transition structure, the α angle is 97.4° (Figure 4), which diverges from the corresponding lower energy conformation of the 2*S*-**1c** allylic alcohol by 19.4° (Figure 3). This divergence will increase the energy of (2*S*,3*S*)-**3c** by 0.3 kcal/mol due to $^{1,2}$A strain (Figure 3a); however, this α angle differs by 57.4° from the ideal *spiro* structure (α 40°). The $\varphi$ angle is 36.2°, which deviates as much as 53.8° from the ideal *spiro* structure. For comparison, the (2*R*,3*S*)-**3c** transition structure possesses an α angle of 46.7°, which differs only 6.2° from the corresponding lower-energy 2*R*-**1c** conformer. This difference increases the energy of (2*R*,3*S*)-**3c** by only 0.1 kcal/mol due to $^{1,3}$A strain. Since the $\varphi$ angle is 72.4°, the α and $\varphi$ values suggest that the (2*R*,3*S*) -**3c** transition structure should be preferred over (2*S*,3*S*)-**3c**. Nevertheless, similar to substrate **1b**, the (2*S*,3*S*)-**3c** is favored by 0.21 kcal/mol in energy in the gas phase (Figure 4) and by 0.70 kcal/mol in $CH_2Cl_2$ (COSMO solvent correction) compared to the (2*R*,3*S*)-**3c** structure. Again, the reason for this is the competition between the $^{1,2}$A and the $^{1,3}$A strain. From the potential energy profiles of the substrates **1a** and **1b** (Figures 1 and 2) we may estimate a destabilization of the (2*R*,3*S*)-**3c** structure caused by $^{1,2}$A and $^{1,3}$A strain to be 1.0 and 2.0 kcal/mol, while for the (2*S*,3*S*)-**3c** structure the balance of competition between $^{1,2}$A and $^{1,3}$A strains amounts to about 1.0 kcal/mol (Figure 3a). Our calculations on the substrates **1a** and **1b** have revealed that $^{1,2}$A strain and the *spiro* electronic effect benefits the *erythro* diastereselectivity, while $^{1,3}$A strain is favorable for *threo* diastereselectivity. Accordingly, we conclude that the higher *threo* diastereselectivity in the epoxidation of substrate **1c** is due to the dominance of the $^{1,3}$A strain, both over $^{1,2}$A strain and the *spiro* electronic effect. Comparison of the substrates **1b** and **1c** discloses that the minimization of $^{1,3}$A strain on the epoxidation of **1c** is counteracted by $^{1,2}$A strain and the *spiro* electronic effect. In addition, solvent effects are also play a role for the diastereoselectivity at the same time. Thus, the *threo* diastereoselectivity of **1c** (*threo:erythro* 83:17) is lower than that of substrate **1b** (*threo:erythro* 91:9).[15c]

Based on above six transition structures **3**, we propose the six product complexes **4** (Scheme 1) for the epoxidation of the three allylic substrates **1**. Geometrical optimization and frequency calculations were performed on these product complexes. The optimized geometries, energies and dipole moments of the products are supplied in the Supporting Information.

**Activation Energies and the *Threo*/*Erythro* Product Ratio.** The energies and entropies for the substrates **1**, prereaction complexes **2**, transition states **3**, and the product complexes **4** are listed in Table S1. The calculated activation energies ($\Delta E^{\ddagger}$), activation enthalpies ($\Delta H^{\ddagger}$), activation free energies ($\Delta G^{\ddagger}$), and solvent correction of the free energies ($\Delta G^{\ddagger}_{solv}$) for the epoxidation of the substrates **1a**−**c** are given in Table 2.

The activation enthalpies ($\Delta H^{\ddagger}$) for these epoxidations range between 13 and 17 kcal/mol. This result is in the range of the available experimental data for metal-catalyzed epoxidations, since it was reported that the activation enthalpies for vanadium catalyzed *tert*-butyl hydroperoxide epoxidation of cyclohexene is 12.7 kcal/

**Table 3. The Calculated Reaction Energies ($\Delta E$), Reaction Enthalpies ($\Delta H$), Reaction Free Energies ($\Delta G$), and Solvent-Corrected Free Energies ($\Delta G_{solv}$) of the Two Lowest-Energy Conformers of Prereaction Complexes 2 to Their *Threo* and *Erythro* Epoxide Products (in kcal/mol)**

| reaction | $\Delta E^a$ | $\Delta H^b$ | $\Delta G^c$ | $\Delta G_{solv}{}^d$ |
|---|---|---|---|---|
| 2*S*-**2a** → (2*S*,3*S*)-**4a** | −42.7 | −42.1 | −43.1 | −43.8 |
| 2*R*-**2a** → (2*R*,3*S*)-**4a** | −45.2 | −43.8 | −43.4 | −49.2 |
| 2*S*-**2b** → (2*S*,3*S*)-**4b** | −43.4 | −42.8 | −42.4 | −42.6 |
| 2*R*-**2b** → (2*R*,3*S*)-**4b** | −44.5 | −43.6 | −40.5 | −42.3 |
| 2*S*-**2c** → (2*S*,3*S*)-**4c** | −45.1 | −44.7 | −45.2 | −45.0 |
| 2*R*-**2c** → (2*R*,3*S*)-**4c** | −44.6 | −46.0 | −43.2 | −44.5 |

[a] Total reaction energies calculated from the total energy in Table S1 of the Supporting Information, $\Delta E = E^{p}_{tot} - E^{r}_{tot}$, where $E^{r}_{tot}$ is the total energy of the prereaction complexes **2** and $E^{p}_{tot}$ is the total energy of the product complexes **4** in Table S1 of the Supporting Information). [b] Gas-phase reaction enthalpy (298 K), $\Delta H = \Delta E + \Delta E_{corr}$, where $\Delta E_{corr}$ is the thermal-correction energy difference between the prereaction complex **2** and the product complex **4** derived from the frequency calculation by the B3LYP/6-31+G(d,p) method. [c] Reaction free energy for change from the prereaction complex **2** to the product complex **4**, which was computed from the frequency results of the B3LYP/6-31+G(d,p) calculations. [d] Difference of the salvation free energy between the prereaction complexes **2** and product complexes **4**, calculated according to the COSMO solvent model from the optimized B3LYP/6-31+G(d,p) structures with the dielectric constant set at $\epsilon$ 8.9 to mimic the $CH_2Cl_2$ medium.

mol and molybdenum catalyzed *tert*-butyl hydroperoxide epoxidation of octane is 18 kcal/mol.[24]

With the solvent-corrected computational activation energies now for the first time available in the Ti(O-*i*-Pr)$_4$/*t*-BuOOH-catalyzed epoxidations of the chiral allylic alcohols **1**, it was important to compute the *threo*:*erythro* product ratios from the above theoretical activation energies and compare them with the experimental data (Scheme 1).[15c,17] Since the epoxidation reactions are subject to the Curtin−Hammett principle, the *threo*:*erythro* product ratio may, therefore, be estimated by eq 1,[17] in which $G_{threo}$ and $G_{erythro}$ are the total free energies that lead to the *threo* and *erythro* products. The calculated solvent-corrected relative activation free energies ($\Delta G_{sol}$) for the *threo* and *erythro* transition structures **3** of the epoxidation for the substrates **1a**−**c** have already been presented in Table 1. According to eq 1 and the solvent-corrected data for $\Delta G_{solv}$ in Table 1, the *threo:erythro* ratio for the epoxidation of substrate **1a** is 12:88, for substrate **1b** it is 92:8, and for substrate **1c** it is 77:23, which are in excellent agreement with the experimental diastereoselectivities in Scheme 1.[15c]

$$\frac{[threo]}{[erythro]} = \frac{\exp(-G_{threo}/RT)}{\exp(-G_{erythro}/RT)} = \exp[-(G_{threo} - G_{erythro})/RT] = \exp(\Delta G/RT) \quad (1)$$

From the computed energy parameters of the prereaction complexes **2** and product complexes **4** (Table S1), we have also estimated the reaction energies, which are listed in Table 3. The heats of formation ($\Delta H$) and free energies ($\Delta G$) of the reactions for the epoxidation of substrates **1** are about −40 kcal/mol (Table 3). Thus, the epoxidation reaction is highly exothermic. This indicates that the *threo:erythro* product ratio is controlled by kinetics of the reactions, as confirmed by the solvent-corrected activation free energies in Table 1.

(24) (a) Gould, E. S.; Hiatt, R. R.; Irwin, K. C. *J. Am. Chem. Soc.* **1968**, *90*, 4573−4579. (b) Baker, T. N.; Mains, G. J.; Sheng, M. N. *J. Org. Chem.* **1973**, *38*, 1145−1148.

## Conclusion

For the epoxidation of the methyl-substituted chiral allylic alcohols by the titanium peroxy complex, we have obtained the optimized structures for the prereaction complexes, transition states, and product complexes involved in the Ti(OH)$_4$/MeOOH (model oxidant) catalyzed oxygen transfer by the density-functional-theory method, B3LYP/6-31+G(d,p). These computations are in good agreement with the experimental activation enthalpies and the diastereoselectivity, the latter expressed by *threo*:*erythro* product ratio. This agreement between the experimental and computational results not only confirms the validity of the Sharpless mechanism for the titanium-catalyzed asymmetric epoxidation,[6] i.e., in the first step is the hydroperoxide-alcohol template is formed, but it also indicates the adequacy of our selected model and computational method. The present DFT computations corroborate that the methyl-labeled chiral allylic alcohols **1a**−**c** may serve as valuable stereochemical probes to elucidate mechanistic fine structure in oxygen-transfer processes. $^{1,2}$A strain and the electronically favored *spiro* transition state dictate *erythro* diastereoselectivity, while $^{1,3}$A strain controls the *threo* diastereoselectivity. When $^{1,3}$A and $^{1,2}$A strain compete, as in the substrate **1c**, the former dominates even at the sacrifice of an idealized *spiro* geometry for the oxygen transfer. In addition, solvent effects are also play a role for the diastereoselectivity at the same time.

**Acknowledgment.** We are grateful to Prof. Y. D. Wu (Hong Kong), Prof. R. D. Bach (USA), and Dr. W. L. Zhu (Singapore) for very helpful discussions. Generous financial support from the National Natural Science Foundation of China (Grant 29725203) and the State Key Program of Basic Research of China (Grant 1998051115) for the work in Shanghai, and the Deutsche Forschungsgemeinschaft (Sonderforschungsprogramm 347, "Selektive Reaktionen metallaktivierter Moleküle") and the Fonds der Chemischen Industrie for the work in Würzburg, is gratefully appreciated The quantum chemical calculations were performed on the Power Challenge R10000 system of the Network Information Center, Chinese Academy of Sciences, Beijing, People's Republic of China.

**Supporting Information Available:** The calculated total energies, thermal correction energies, entropies, and solvent-effect corrections are available in Table S1. The structures, relative energies, and dipole moments of these prereaction complexes and products are shown in Figures S1 and S2, respectively. The Cartesian coordinates of the all calculated structures are also included. This material is available free of charge via the Internet at http://pubs.acs.org.

JO016015C